Renewable Energy 138 (2019) 820–832

Contents lists available at ScienceDirect

Renewable Energy

journal homepage: www.elsevier.com/locate/renene

Olefin oligomerisation over nanocrystalline MFI-based micro/mesoporous zeotypes synthesised via bottom-up approaches

Andreia F. Silva [a], Auguste Fernandes [b], Margarida M. Antunes [a], Maria F. Ribeiro [b], Carlos M. Silva [a], Anabela A. Valente [a, *]

[a] CICECO - Aveiro Institute of Materials, Department of Chemistry, University of Aveiro, Campus Universitário de Santiago, 3810-193 Aveiro, Portugal
[b] Institute for Biotechnology and Bioengineering, Centre for Biological and Chemical Engineering, Instituto Superior Técnico, Av. Rovisco Pais, 1049-001 Lisboa, Portugal

ARTICLE INFO

Article history:
Received 12 July 2018
Received in revised form
5 November 2018
Accepted 5 February 2019
Available online 6 February 2019

Keywords:
1-Butene
Oligomerisation
Continuous-flow
MFI topology
Hierarchical zeotypes
Hydrothermal synthesis

ABSTRACT

The oligomerisation of 1-butene was studied under high-pressure continuous-flow conditions (200–250 °C, 30–40 bar), in the presence of micro/mesoporous zeotypes based on the MFI topology, which were prepared via different non-destructive bottom-up strategies: crystallization of silanized protozeolitic units; co-templating with a dual function (polymeric) template; and using a sole structure directing agent (non-surfactant and non-polymeric) to generate mesoporosity. The synthesis method influenced the material properties and consequently the catalytic performance. In targeting hydrocarbons with boiling point ranges characteristics of diesel, the zeotypes benefited from regular morphology, reduced crystallite size, mesoporosity and enhanced molar ratio of Lewis (L) to Brønsted (B) acid sites (L/B). In general, the zeotypes outperformed commercial zeolite ZSM-5. The best-performing zeotype was prepared according to the Serrano strategy based on the crystallization of silanized zeolitic seeds, and led to 97% conversion and an average space-time yield of liquid products of 1077 mg g_{cat}^{-1} h^{-1}, at 250 °C, 40 bar. The zeotypes seemed more stable than the commercial zeolite, based on molecular level characterization studies of the used/regenerated catalysts, with some differences in catalytic activity.

1. Introduction

The importance of developing and implementing efficient and clean processes for fuel production is evident in an energy-expanding world. Worldwide, transportation is largely based on petroleum and other liquid fuels obtained from natural gas, coal, or biofuels [1,2]. Projections for 2040 based on the International Energy Outlook 2016 [1] indicate that gasoline (33%) and diesel/biodiesel (33%) remain the largest transportation fuels, followed by jet fuel (14%), with the remaining 9% regarding electricity, residual fuel oil and other liquids. The great dependence of society on fossil fuels is believed to contribute to global warming, and in mitigating this problem, the solutions may involve the use of renewable sources of energy, and repurposing industrial byproducts for the production of chemicals and fuels.

Light olefins are byproducts of petrochemical or Fischer-Tropsch processes [3–6], and, on the other hand, may be obtained from renewable sources, e.g. butenes from carbohydrate biomass [7–9]. The oligomerisation of light olefins (C2-C5) may be a flexible technology and attractive route to produce diverse products including synthetic transportation fuels (gasoline, diesel, jet fuel) with reduced content of sulphur and aromatic compounds, drugs, detergents, lubricants and dyes [10,11]. Olefin oligomerisation is favoured in the presence of acid catalysts, which should be adequate for continuous-flow processes. In this sense, porous solids possessing significant specific surface area available for the catalytic reaction, are attractive. On the other hand, olefin oligomerisation involves the formation of relatively bulky products, and, thus, to facilitate mass transport and maximize the portion of effectively utilized catalyst in the process, it is desirable that the solid acids possess sufficiently large pores [12–16].

Important industrial solid acid catalysts are porous aluminosilicates. This category of materials is very versatile: amorphous or

* Corresponding author.
E-mail address: atav@ua.pt (A.A. Valente).

https://doi.org/10.1016/j.renene.2019.02.019
0960-1481/

crystalline materials with different topologies, morphological, textural and acid properties may be prepared [17–19]. Most successful types of aluminosilicates applied in the industry include zeolites, which are crystalline and microporous materials. Zeolites may possess superior acid properties (e.g. stronger acidity) to amorphous aluminosilicates such as, ordered mesoporous materials of the type MCM-41, SBA-15 or TUD-1; the latter possess less rigid frameworks and silanol surface groups, albeit larger pores than zeolites, advantageously allowing enhanced acid sites accessibility [4,20–24]. Favourable compromise between textural and acid properties of porous solid acids is important for maximizing product yields. Another important factor for maximizing catalyst productivity is the catalyst stability. Zeolites possessing the MFI topology (medium pore, with the channel sizes of $0.55 \times 0.51\ nm^2$ and $0.56 \times 0.53\ nm^2$) are relatively robust industrial catalysts [25,26] and used in commercial olefin oligomerisation processes [27–31]. However, they may present important mass transfer limitations and suffer fast catalyst deactivation in the oligomerisation of olefins such as butene [32]. Hence, great attention has been drawn to the development of aluminosilicate zeotypes with reduced crystallite sizes and/or enlarged pores. The synthetic strategies for obtaining zeotypes possessing mesoporosity may be classified as top-down or bottom-up approaches [33–36]. Zeotypes prepared via top-down approaches were studied for olefin oligomerisation, and possessed superior performances in comparison to conventional microporous zeolites; the zeotypes were based on the MFI [37–39], MOR [40,41], FAU [42] and TON [43] topologies.

A main difference between the top-down and bottom-up approaches is that the former may be somewhat destructive compared to the latter. Regarding the bottom-up approaches, several specific strategies (e.g. with or without addition of structure-directing agents) were reported for preparing zeotypes based on different topologies and possessing mesoporosity (2–50 nm). Wang et al. [44] and Yang et al. [45] reported the synthesis of hydrothermally stable zeotypes based on the MFI topology, via a (soft) co-templating protocol (denoted CoT), which involved the simultaneous use of small and large cationic ammonium-based hydrophilic templates. The mesoporosity could be fine-tuned by changing the amount of the large cationic template [44,45]. Serrano et al. [46–48] reported a strategy (denoted PZSi) based on the crystallization of silanized zeolitic seeds (or protozeolitic units) possessing MFI topology, which may be followed by a treatment with a basic surfactant-containing solution (PZSiS) to rearrange the zeolitic units over the mesopore surface. Wan et al. [49] reported a method not requiring additional template or zeolite seeding crystals (denoted noT). The hierarchical zeotypes presented superior performances to conventional microporous ZSM-5 for different acid-catalysed liquid or gas phase reactions, under batch or continuous-flow operation. In particular, the synthetic approach by Wan et al. [49] led to porous solid acids that enhanced the conversion of methanol to gasoline, and was more stable towards coking.

In this work, the oligomerisation of 1-butene was studied under continuous-flow, and relatively high-pressure conditions (characteristic of industrial olefin oligomerisation processes [27–31], favouring the formation of oligomers which involves reduction of the total number of moles of the system), in the presence of zeotypes based on the MFI topology and possessing mesoporosity. The zeotypes were prepared via different bottom-up approaches, based on the strategies CoT, PZSi, PSZiS and noT referred above. The zeotype catalysts were benchmarked (at 200 °C, 30 bar) with commercial zeolite ZSM-5 possessing Si/Al ratio intermediate of the zeotypes (Si/Al in the range 20–51). Special attention was given to aspects of catalyst stability.

2. Experimental

2.1. Materials

All reagents and solvents were obtained from commercial sources and used as received. For materials syntheses: aluminium (III) isopropoxide (AiP; 98%, Aldrich), sodium aluminate (50–56% Al_2O_3, Riedel de Haen), tetraethylorthosilicate (TEOS; 98%, Sigma), tetrapropylammonium hydroxide solution (TPAOH; 40 wt% in water, Alfa-Aesar), sodium hydroxide (97%, Sigma-Aldrich), poly(-acrylamide-co-diallyldimethylammonium chloride) (PDD-AM; 10% in water, Aldrich), [3-(phenylamino)propyl]trimethoxysilane (PHAPTMS; Aldrich), hexadecyltrimethylammonium bromide (CTAB; 98%, Aldrich), ammonium hydroxide (28–30%, Sigma-Aldrich), and ammonium nitrate (98%, Aldrich).

For the catalytic tests: 1-butene (99.6%, Praxair), nitrogen (Air Liquide), silicon carbide (SiC, Ø 0.31 mm, SIKA), dichloromethane (analytical reagent grade, Fisher Chemical), and *n*-pentane (95%, Fluka).

The commercial zeolite NH_4ZSM-5 (as reference, the molar ratio Si/Al is 25, and the specific surface area equals $425\ m^2\ g^{-1}$, Alfa-Aesar) was tested as benchmark catalyst after calcination at 550 °C (heating rate of 1 °C min^{-1}) in static air during 5 h. The calcined material is denoted ZSM-5(29) where 29 is the molar ratio Si/Al determined by EDS (discussed ahead).

2.2. Syntheses of the catalysts

The zeotype materials based on the MFI topology were synthesised via bottom-up approaches, and the prepared materials were denoted as hZSM-5(x)-y, where x is the Si/Al ratio giving by EDS, and y is the abbreviation of the synthesis method. The synthesis protocols were adapted from the literature [44,46,49]. The protocols/conditions of the synthesised zeotypes are summarised in Table 1.

2.2.1. Catalyst hZSM-5(31)-noT

The free template method was carried out following a similar procedure to that described by Wan et al. [49] Specifically, 0.33 mmol of $NaAlO_2$, 12.7 mmol of TPAOH solution (40% in H_2O) and 2148 mmol of milliQ-water were mixed and stirred at room temperature for 30 min. Then, 32.9 mmol of TEOS was added dropwise. The molar composition of the synthesis-gel was $1Al_2O_3$: $101SiO_2$: $1.34Na_2O$: 39TPAOH: 7215 H_2O. The resulting mixture was stirred at room temperature for 22 h in order to obtain a uniform gel, followed by crystallization at 180 °C for 48 h in a PTFE-lined stainless-steel autoclave, under static, hydrothermal conditions. After cooling, the resultant product was recovered by centrifugation, washed thoroughly with milliQ-water and dried at 100 °C overnight. The solid was gently grinded using an Agate mortar and pestle, and calcined at 550 °C in static air for 5 h (heating rate of 1 °C min^{-1}). The protonic form was obtained by ion-exchange with 1.0 M NH_4NO_3 aqueous solution (1 g of calcined sample per 10 mL of solution), at 50 °C, under stirring. The solution was renewed two times, every 24 h. Finally, the solid was centrifuged, washed with milliQ water, dried at 100 °C over-night, and calcined at 500 °C in static air for 5 h (heating rate of 1 °C min^{-1}), giving a material denoted hZSM-5(31)-noT (noT stands for no additional template).

2.2.2. Catalysts hZSM-5(x)-PZSi and hZSM-5(47)-PZSiS

The method of silanization of protozeolitic units was employed following a similar procedure to that described by Serrano et al. [46] Specifically, the precursor ZSM-5 solution was prepared by mixing 8.11 mmol of TPAOH, 928 mmol of milliQ-water, 42.3 mmol of TEOS and 0.71 mmol of AiP for hZSM-5(51)-PZSi or 1.41 mmol of

Table 1
Protocols and synthesis conditions of the zeotypes based on the MFI topology.

Synthesis step	noT	PZSi	CoT
Synthesis mixture	TEOS, TPAOH[a], $NaAlO_2$, H_2O (50)[b]	TEOS, TPAOH, AiP, H_2O (30 and 60)[b]	TEOS, TPAOH, $NaAlO_2$, H_2O (36)[b]
Aging (with stirring)	20 h, aT[c]	44 h/aT[c]; 22 h/90 °C	3 h, 100 °C
Additional template	None	PHAPTMS, 90 °C/6 h	PDD-AM, aT[c]/15 h
Hydrothermal treatment	180 °C, 2 d[d], static	170 °C, 7.7 d[d], static	180 °C, 6 d[d], static
Centrifugation, wash, dry	100 °C	110 °C	100 °C
Calcination	550 °C/5 h	550 °C/5 h	550 °C/5 h
Ion-exchange; calcination	(3×) 1.0 M NH_4NO_3, 50 °C/24 h; 500 °C/5 h	None	(3×) 1.0 M NH_4NO_3, 80 °C/2 h; 550 °C/4 h
Sample name	hZSM-5(31)-noT	hZSM-5(x)-PZSi[e]	hZSM-5(31)-CoT

[a] TPAOH as the structure-directing agent accounting for the hierarchical features.
[b] Si/Al ratio of the synthesis gel.
[c] aT = ambient temperature.
[d] d = days.
[e] x is the molar ratio Si/Al of the final material (x = 20 or 51).

AiP for hZSM-5(20)-PZSi; the molar composition of the synthesis-gel was $1Al_2O_3$: $120SiO_2$: 23TPAOH: 3000 H_2O for hZSM-5(51)-PZSi and $1Al_2O_3$: $60SiO_2$: 11.5TPAOH: 1500 H_2O for hZSM-5(20)-PZSi. For the two materials, the mixture was aged at room temperature for 44 h and precrystallized under reflux and stirring (100 rpm) at 90 °C for 22 h. The resulting protozeolitic units were functionalized using 8 mol% of PHAPTMS (with respect to the silica content in the initial gel), and the silanization reaction was performed at 90 °C for 6 h, under reflux, followed by crystallization at 170 °C for 184–186 h in a PTFE-lined stainless-steel autoclave, under static, hydrothermal conditions. After cooling, the resultant product was recovered by centrifugation, washed thoroughly with milliQ-water and dried at 110 °C overnight. The solid was gently grinded using an Agate mortar and pestle, and calcined at 550 °C in static air for 5 h (heating rate of 1 °C min^{-1}), giving a material denoted hZSM-5(x)-PZSi (PZSi stands for ProtoZeolitic units subjected to Silanization), where x stands for the Si/Al ratio of the synthesis gel.

The resulting hZSM-5(51)-PZSi material was submitted to a mesopore narrowing treatment. Specifically, 1.0 g of material was dispersed in 62.8 g of a 0.37 M NH_4OH aqueous solution containing 0.7 g of CTAB. The resulting mixture was stirred at room temperature for 30 min, and then subjected to a hydrothermal treatment under static conditions, for 20 h at 150 °C in a PTFE-lined stainless-steel autoclave. The resultant product was recovered by centrifugation, washed thoroughly with milliQ-water and dried at 110 °C overnight. The solid was gently grinded using an Agate mortar and pestle, and calcined at 550 °C in static air for 5 h (heating rate of 1 °C min^{-1}), giving a material denoted hZSM-5(47)-PZSiS (PZSiS stands for ProtoZeolitic units subjected to Silanization, followed by Surfactant treatment). This protocol does not require ion-exchange since no alkaline source is used.

2.2.3. Sample hZSM-5(31)-CoT

The co-templating method was carried out following a similar procedure to that described by Wang et al. [44]. Specifically, 0.43 mmol of $NaAlO_2$, 9.8 mmol of TPAOH and 31.0 mmol of TEOS were mixed with 1268 mmol of milliQ-water under stirring and aged at 100 °C for 3 h. Then, 3.0 mmol of PDD-AM were added into the reaction mixture. The molar composition of the synthesis-gel was $1Al_2O_3$: $72SiO_2$: 1.3 Na_2O: 23TPAOH: 4000 H_2O. The mixture was stirred for 15–16 h at room temperature, and then was transferred into a PTFE-lined stainless-steel autoclave for crystallization at 180 °C for 144 h. The resulting product was collected by centrifugation, washed thoroughly with milliQ-water and dried at 100 °C overnight. The solid was gently grinded using an Agate mortar and pestle, and calcined at 550 °C in static air for 5 h (heating rate of 1 °C min^{-1}). The protonic form was obtained by ion-exchange with 1.0 M NH_4NO_3 aqueous solution (1 g of calcined sample per 10 mL of solution), at 80 °C, under stirring. The solution was renewed three times, every 2 h. Finally, the solid was centrifuged, washed with milliQ water, dried at 100 °C over-night, and calcined at 550 °C in static air for 4 h (heating rate of 1 °C min^{-1}), giving a material denoted hZSM-5(31)-CoT (CoT stands for co-template).

2.3. Characterization of the catalysts

The PXRD data were collected on an Empyrean PANalytical diffractometer ($Cu_{K\alpha}$ X-radiation, $\lambda = 1.54060$ Å) in a Bragg-Brentano para-focusing optics configuration (45 kV, 40 mA). Samples were prepared in a spinning flat plate sample holder and step-scanned in the range from 3 to 70° (2θ) with steps of 0.026°. A PIXEL linear detector with an active area of 1.7462° was used with a counting time of 68 s per step. The low angle (0.5–5° 2θ) PXRD data were collected using the transmission mode, and with the sample deposited between Mylar foils; the samples were step-scanned in 0.01° 2θ steps with a counting time of 80 s per linear detector active area of 2.0°.

SEM images, EDS analysis and elemental mappings (Al, Si) were obtained on a Hitachi SU-70 SEM microscope with a Bruker Quantax 400 detector operating at 20 kV. TEM was performed on a Hitachi HD2700 instrument, and the samples were prepared by spotting carbon-film-coated 400 mesh copper grids (Agar Scientific) with a suspension of the solid sample in ethanol.

Nitrogen adsorption-desorption isotherms were measured at 196 °C, using a Quantachrome instrument (automated gas sorption data using Autosorb IQ_2). The samples were pre-treated at 300 °C for 3 h, under vacuum (3 Torr). The external or mesopore surface area ($S_{ext,\ meso}$) and micropore volume (V_{micro}), were calculated by the t-plot method. The pore size distributions (D_p) were determined by the DFT method (adsorption branch). Differential scanning calorimetry analyses (DSC) were performed under air, from room temperature until 800 °C, with a heating rate of 10 °C min^{-1}, using a Shimadzu DSC-50 instrument.

The ^{27}Al MAS NMR spectra were recorded at 182.432 MHz using a Bruker Avance 700 (16.4 T) spectrometer with a unique pulse, a recycle delay of 1 s and a spinning rate of 14 kHz. The acid properties were measured using a NexusThermo Nicolet apparatus (64 scans and resolution of 4 cm^{-1}) equipped with a home-made vacuum cell, using self-supported discs (5–10 mg cm^{-2}) and pyridine as the basic probe. After in situ outgassing at 450 °C for 3 h (10^{-6} mbar), pyridine (99.99%) was contacted with the sample at 200 °C for 10 min and subsequently evacuated at the same temperature or at 450 °C for 30 min, under vacuum (10^{-6} mbar). The IR

bands at ≈1540 and 1455 cm^{-1}, which are related to pyridine adsorbed on Brønsted (B) and Lewis (L) acid sites, respectively, were used for quantification [50]. The total amount of acid sites (L + B) and the molar ratios L/B were determined at the lowest desorption temperature (200 °C). The amount of strong acid sites was evaluated by the molar ratios B_{450}/B_{200} (B acid strength) and L_{450}/L_{200} (L acid strength), respectively, where L_T and B_T are the amount of L and B acid sites, respectively, which remained in the solid material after evacuation at $T = 450$ or 200 °C.

2.4. Catalytic tests

The catalytic oligomerisation of 1-butene ($1C_4$) was carried out under continuous-flow, high-pressure conditions, using a stainless steel, fixed-bed reactor (10 mm internal diameter). A simplified representation of the experimental setup is given in Fig. 1, indicating the equipment used for controlling the feed flow rate (for $1C_4$, a syringe pump Chemyx, model Nexus 6000; and for N_2, a gas mass flow controller Bronkhorst, EL-FLOW), pressure (backpressure regulator located after the reactor; Equilibar, LF-Primary Research Series) and temperature (furnace (Termolab), temperature controller and thermocouple located inside the reactor). The reactor was loaded with catalyst (150 mg) and silicon carbide (diluent to enable a uniform temperature distribution along the catalytic bed); the total bed volume was ≈1.8 cm^3. The catalysts were activated at 450 °C for 3 h under nitrogen flow (10 cm^3 min^{-1}) prior to the catalytic reaction. Subsequently, the reactor temperature was set to the desired catalytic reaction temperature, and the olefin was fed using nitrogen as the carrier gas (molar ratio of $1C_4$:N_2 = 15:85).

The gas phase (non-condensed compounds) was sampled in regular intervals of ≈1 h, for a time-on-stream (TOS) of ≈7 h, using loops (heated at 200 °C) which were connected on-line to the Master Fast GC gas chromatograph (DANI) equipped with a capillary column (ValcoBond VB-1, 60 m × 0.25 mm x 1.50 μm), FID detector, and a split/splitless injector. Quantifications were based on external calibration curves using pure $1C_4$; the experimental range of error was less than 5%. The catalytic results were expressed as conversion of butenes (X_{C4}) which did not react to give higher molar mass products using the equation $X_{C4}\,(\%) = \frac{F_{1C4in} - F_{C4out}}{F_{1C4in}} \times 100$, where F_{1C4in} is the inlet molar flow rate of 1-butene, and F_{C4out} is the outlet molar flow rate of butenes. The values of X_{C4} correspond to the conversion at ≈7 h on-stream, excluding the values presented as a function of TOS where X_{C4} is calculated for each point (Fig. S5).

The liquid reaction products were condensed in a jacketed cooling trap (cooling fluid at 5 °C; pressure inside the trap was ≈1 bar), and the mixture was analysed using the same GC

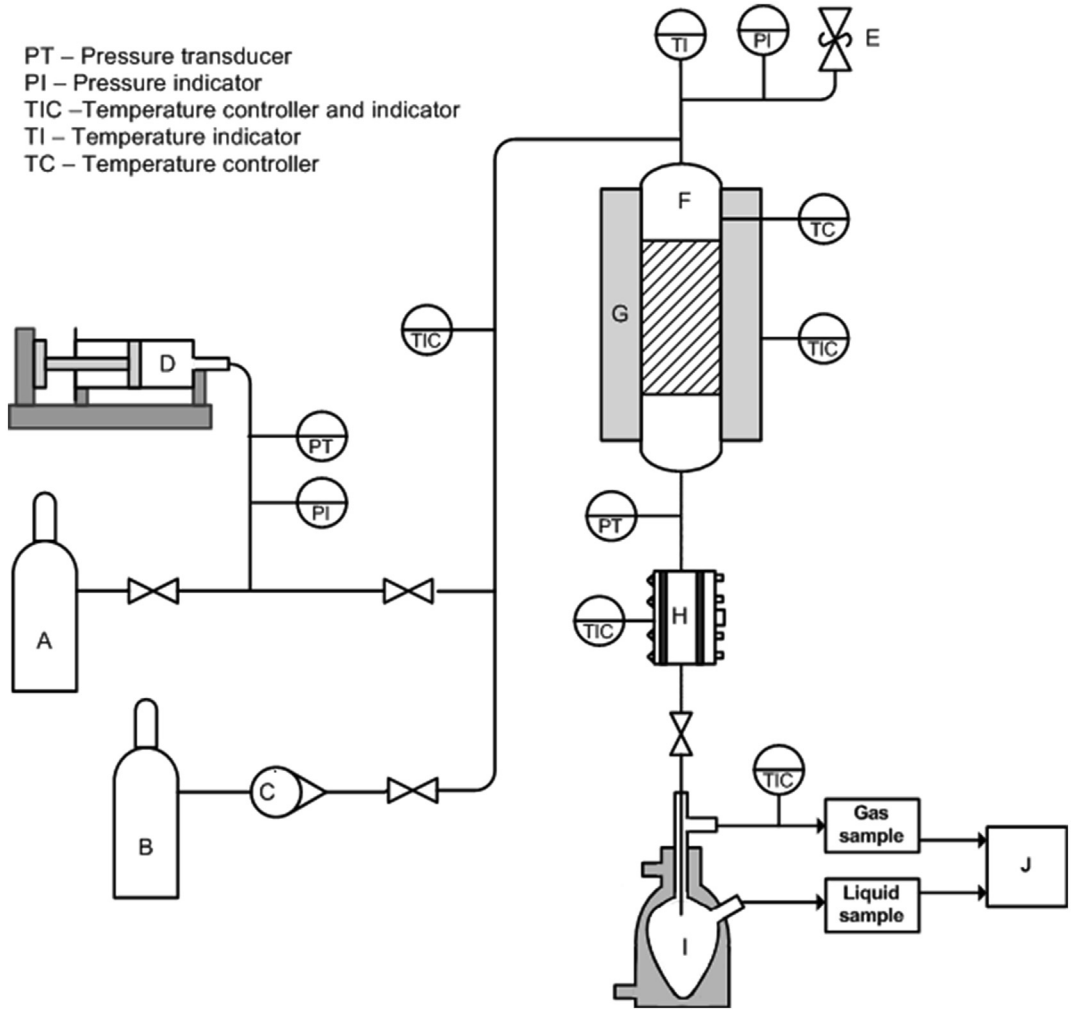

Fig. 1. Flow diagram of the lab-scale catalytic reactor setup. A – 1-Butene cylinder, B – Nitrogen cylinder, C - Mass flow controller, D - Syringe pump, E – Relief valve (Parker), F - Fixed-bed reactor, G - Tubular oven, H - Back-pressure regulator, I - Jacketed cooling trap, J - Gas chromatograph.

instrument; concentrations were based on calibrations using ASTM D2887 Quantitative Calibration mixture (*n*-alkanes C_6-C_{44}), and internal standard. The products lump distributions (PLD) curves correspond to the products formed during ≈7 h TOS. These curves are represent the set of values of selectivity ($S_{C[y-z]}$) towards a lump of compounds possessing y to z number of carbon atoms per molecule (lump $C_{[y-z]}$, where z > y), which was calculated using the equation $S_{C[y-z]}\,(\%) = \frac{n_{C[y-z]}}{\sum n_{C[y-z]}} \times 100$, where $n_{C[y-z]}$ is the moles for product lump $C_{[y-z]}$, and $\sum n_{C[y-z]}$ is the total moles of products in the range C_6-C_{24}. The fractions corresponding to the 170 °C cut characteristic of naphtha products (NCut), and to the 170–390 °C cut characteristic of diesel products (DCut, corresponding approximately to the C_{10}-C_{24} *n*-paraffinic range) were determined according to the ASTM D2887 method (Standard Test Method for Boiling Range Distribution of Petroleum Fractions by Gas Chromatography) [37,43,51]. These analyses were validated using the ASTM D2887 Reference Gas Oil nº 1 (Supelco, sample 1, Batch 2) and the results agreed, within the allowable difference ranges, with the ASTM D2887 consensus boiling point values. It is worth mentioning that C_{10} type products (based on the temperature cut point) may be distributed between the DCut and NCut fractions. The average space time yields (STY, expressed as mg g_{cat}^{-1} h^{-1}) were based on the mass fractions of DCut and NCut of total liquid (condensed) products formed during ≈7 h TOS. In general, the material balances closed in at least 85%. The catalytic performances were compared based on X_{C4} and STYs considering approximately steady-state conditions within ≈7 h TOS.

The spent catalysts were thermally treated at 550 °C (1 °C min^{-1}) for 6 h, to burn-off carbonaceous matter, giving the recovered solids, which were characterised or used for catalytic tests. Details regarding the determination of the cetane number (CN, based on ^{1}H NMR spectroscopy), isoparaffinic index (I, based on ^{1}H NMR spectroscopy), aromatics content (%Ar, based on ^{1}H NMR spectroscopy) of the reaction products, the amount of coke (based on elemental analysis) present in the spent catalysts, and checking for operation under kinetic regime, are given in the Supplementary Material.

3. Results and discussion

3.1. Characterization of the catalysts

Micro/mesoporous materials based on the MFI topology were prepared via bottom-up approaches, under hydrothermal conditions. The MFI features of the materials prepared were ascertained by PXRD diffraction, which showed the characteristic reflections in the range 7–57° 2θ, with the most intense peaks at 7-8° and 23-24° 2θ (Fig. 2) [52,53]. Low angle PXRD showed a broad peak in the range 0.5–1.5° 2θ, likely associated with the mesoporous features of the zeotypes prepared (Fig. S1).

Fig. 3 shows the SEM and STEM images of the zeotypes. The noT and the PZSi(S) protocols led to materials consisting of pseudo-spherical aggregates (≈200–400 nm in size, Fig. 3-a,d,g,j) of nanocrystallites (≈10–60 nm, Fig. 3-c,f,i,l), somewhat in agreement with literature data for similarly prepared materials [46,49]. The PZSiS protocol involving a final surfactant treatment seemed to lead to some coalescence (Fig. 3-k), forming larger nanocrystallites of ≈30–60 nm compared to ≈10–20 nm for PZSi. The CoT protocol led to irregular aggregates (ca. 1–1.5 μm) of nanocrystallites (≈30–40 nm), Fig. 3-m,n,o. Commercial ZSM-5 zeolite (ZSM-5(29)) consists of small microcrystals (100–300 nm, Fig. 3-p,q,r). EDS (Table 2) and Si and Al mappings (Fig. S2) suggested that the materials possessed uniform dispersions of metal/metalloid surface species, and the molar ratios Si/Al were in the range 20–51 (Table 2).

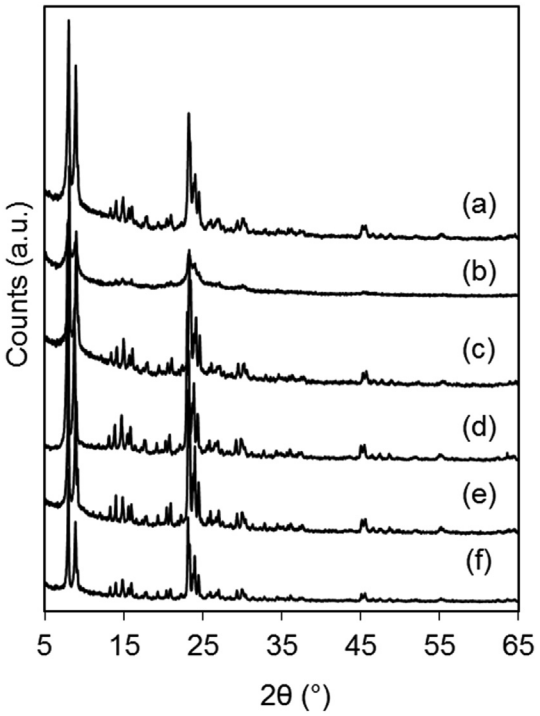

Fig. 2. PXRD patterns for hZSM-5(31)-noT (a), hZSM-5(20)-PZSi (b), hZSM-5(51)-PZSi (c), hZSM-5(47)-PZSiS (d), hZSM-5(31)-CoT (e), and ZSM-5(29) (f).

The materials possessed BET specific surface area (S_{BET}) in the range 308–853 m^2g^{-1} (Table 2), and both micro- and mesoporosity (micropore sizes of 0.55–0.57 nm, and mesopore sizes of 2–10 nm, Fig. 4). For the prepared zeotypes excluding hZSM-5(31)-CoT, the portion of specific mesopore surface area (S_{meso}) was in the range 43–59%, and that of micropore volume was 7–12%. The material hZSM-5(31)-CoT possessed highest S_{BET} (853 $m^2\,g^{-1}$), albeit the portion of microporous volume was considerable (52%). The commercial zeolite ZSM-5(29) possessed the lowest S_{meso}.

FT-IR spectroscopy of the dehydrated materials (self-supported samples) showed a band centered at ca. 3743 cm^{-1}, and a shoulder at ca. 3730 cm^{-1}, which seemed more pronounced for the zeotypes than zeolite ZSM-5(29) (Figs. S3–A). The band at ca. 3743 cm^{-1} is assignable to the OH stretching vibration of isolated silanol groups, and that at ca. 3730 cm^{-1} may be due to weakly perturbed silanol groups (e.g. defect sites) [54,55].

The materials were characterised at the molecular level by ^{27}Al MAS NMR spectroscopy to identify the types of Al species, and FT-IR spectroscopy using pyridine as base probe to investigate the surface acidity. ^{27}Al MAS NMR spectroscopy indicated that all materials exhibited a main resonance centered at ca. 55 ppm assignable to four-coordinated (framework) aluminum species (Al_{tetra}), and a small resonance at ca. 0 ppm assignable to six-coordinated Al species (Al_{octa}) which may be bonded or not to the framework (Fig. S4, Table 3) [56]. The ratio Al_{tetra}/Al_{octa} (determined via deconvolution of the spectra and integration of the peaks) were in the range 3–13 for the zeotypes and 16 for zeolite ZSM-5(29). The lower Al_{tetra}/Al_{octa} together with the above FT-IR spectroscopic results for the zeotypes, suggest that these may possess more defect sites than the zeolite, which may be partly associated with the reduced crystallite sizes of the zeotypes.

The acid properties measured by FT-IR spectroscopy of adsorbed pyridine (base probe) are indicated in Table 3. All materials exhibited bands at ≈1540 and 1455 cm^{-1} assigned to Brønsted and

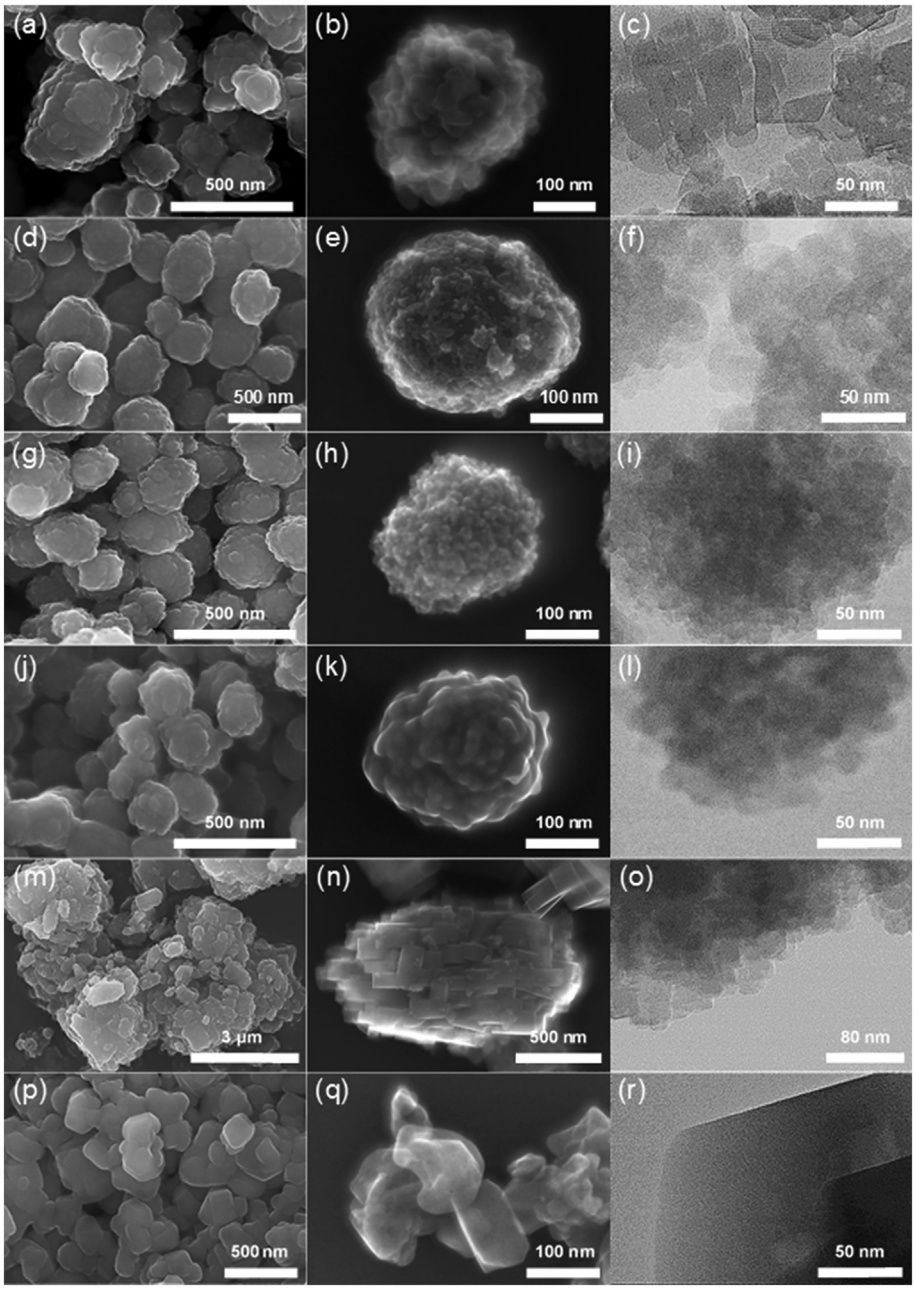

Fig. 3. SEM (left column, a,d,g,j,m,p) and STEM (middle and right columns) images of hZSM-5(31)-noT (a, b, c), hZSM-5(20)-PZSi (d, e, f), hZSM-5(51)-PZSi (g, h, i), hZSM-5(47)-PZSiS (j, k, l), hZSM-5(31)-CoT (m, n, o), and ZSM-5(29) (p, q, r).

Table 2
Elemental analyses and textural properties of the MFI-based materials.[a]

Sample	Si/Al[a]	Textural properties						
		S_{BET} (m^2g^{-1})	S_{meso}[b] (m^2g^{-1})	$\%S_{meso}$	V_p (cm^3g^{-1})	V_{micro}[c] (cm^3g^{-1})	$\%V_{micro}$	D_p[d] (nm)
hZSM-5(31)-noT	31	308	168	54	0.46	0.04	8	2–10
hZSM-5(20)-PZSi	20	721	308	43	0.74	0.09	12	2–5
hZSM-5(51)-PZSi	51	558	289	52	0.77	0.07	10	2–7
hZSM-5(47)-PZSiS	47	464	275	59	0.76	0.05	7	2–5
hZSM-5(31)-CoT	31	853	140	16	0.48	0.25	52	2–5
ZSM-5(29)	29	334	97	29	0.47	0.17	36	–

[a] Molar ratio determined by EDS.
[b] External/mesoporous specific surface area.
[c] Micropore volume (calculated for $p/p_0 \approx 0.99$).
[d] Mesopore size range. For all materials, the micropore size distribution (based on DFT) indicated a median pore size in the range 0.55–0.57 nm.

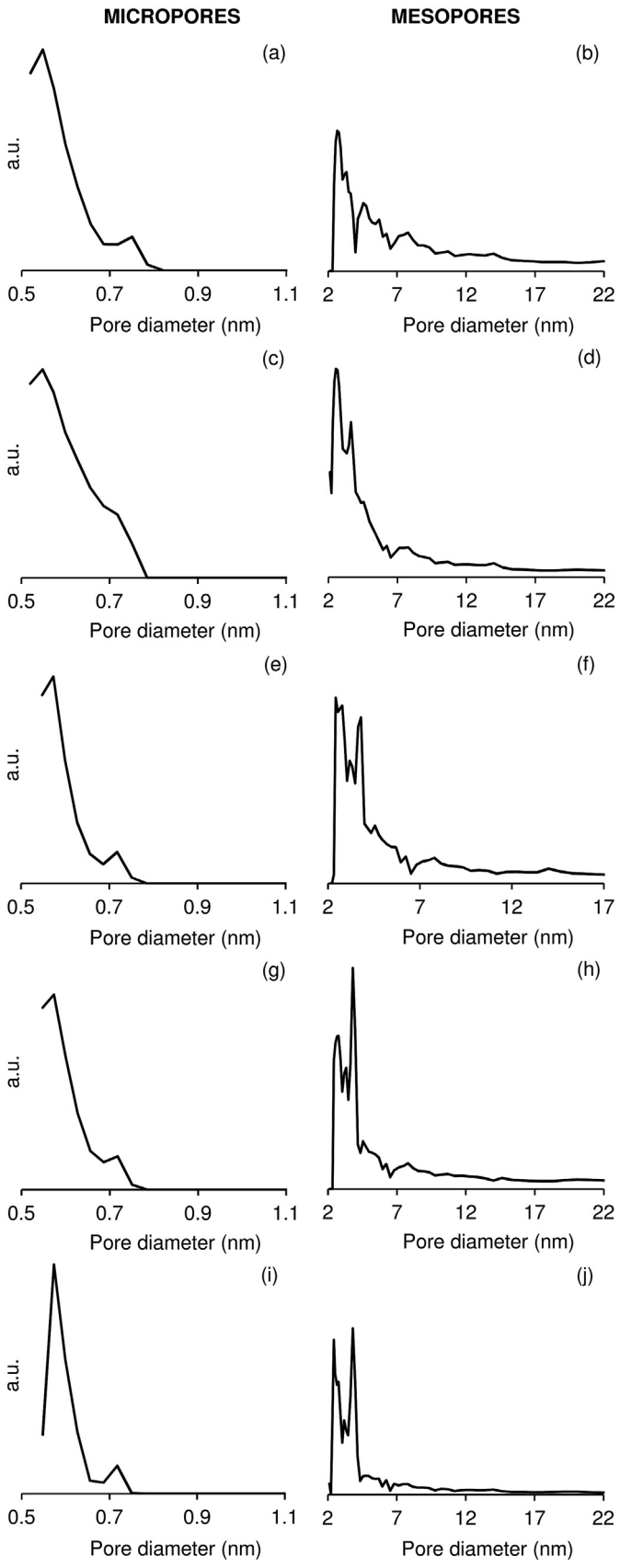

Fig. 4. Pore size distribution curves (DFT method) for hZSM-5(31)-noT (a, b), hZSM-5(20)-PZSi (c, d), hZSM-5(51)-PZSi (e, f), hZSM-5(47)-PZSiS (g, h), and hZSM-5(31)-CoT (i, j).

Lewis acid sites (Fig. S3–B) [50]. In general, the zeotypes and zeolite ZSM5(29) possessed essentially strong Lewis acid sites (L_{450}/L_{200} in the range ~0.5–1) and weak/moderate Brønsted acidity ($B_{450}/B_{200} < 0.3$) (Table 3). Zeolite ZSM-5(29) possessed the higher amount of total acid sites (L + B) than the zeotypes. Of the zeotypes, hZSM-5(31)-noT and hZSM-5(20)-PZSi possessed highest (and similar) L + B (251–252 μmol g^{-1}). The noT and CoT protocols gave materials possessing comparable or stronger acidity to zeolite ZSM-5(29), whereas the PZSi protocol gave materials possessing weaker acidity. Changing the Si/Al ratio of the materials prepared via the PZSi protocol influenced L + B and the molar ratio L/B, without affecting significantly the acid strength; L + B and L/B increased with decreasing Si/Al ratio (Table 3). The zeotype hZSM-5(20)-PZSi possessed the highest molar ratio L/B of 1.3, compared to < 0.6 for the remaining materials.

3.2. Catalytic oligomerisation

3.2.1. General considerations

The MFI-based materials prepared via the bottom-up synthetic approaches were tested for the oligomerisation of 1-butene (1C4), under high-pressure (30 bar) continuous-flow conditions, at 200 °C, and weight hourly space velocity (WHSV) of 2.2 $g_{1C4}\ g_{cat}^{-1}\ h^{-1}$. Previous studies using Beta type catalysts (and the same reactor setup) indicated that these conditions were a reasonable compromise for targeting diesel cut products with low aromatics content, operating under kinetic regime [57]. WHSV of 2.2 $g_{1C4}\ g_{cat}^{-1}\ h^{-1}$ somewhat lies in the range of values of WHSV for olefin oligomerisation technologies such as, Mobil Olefins to Gasoline and Distillate (MOGD; WHSV of 0.5–2 h^{-1} [58,59]). All materials prepared were effective in converting 1-butene (1C4) to higher molar mass products. The gaseous effluent stream contained essentially unreacted 1C4 and its isomers *cis*-2-butene and *trans*-2-butene. The conversion of total butenes (X_{C4}) was in the range 27–77% (Fig. 5). For all catalysts, the molar ratio of (C4 isomer products):1C4 was in the range 5.0–5.7, and the ratio of cis:trans isomers was ca. 0.6. The predominance of the trans C4 isomer is in agreement with literature data for the isomerisation of 1C4 [60]. The isomer distributions with chains of a given size may be independent of the type of solid acid catalyst, and correspond to thermodynamic equilibrium compositions [61]. On the other hand, alkenes possessing terminal C=C bonds may undergo faster oligomerisation than alkenes possessing internal C=C bonds [62,63], contributing to the predominance of the internal C4 isomers over 1C4.

The liquid product lump distribution (PLD) curves corresponded to products possessing number of carbon atoms in the range C6-C24, i.e. products with boiling point ranges corresponding to the 170 °C cut (C_6-C_{10}) characteristic of naphtha type products (NCut), and the 170–390 °C cut (C_{10}-C_{24}) characteristic of diesel type products (DCut) (Fig. 6). A comparative study for all materials indicated that the zeotypes possessed different catalytic activities and led to different average space-time yields of liquid products (STY). Higher catalytic activity seemed accompanied by a greater production of higher molar mass products (Fig. 7). In general, the zeotypes performed superiorly to commercial zeolite ZSM-5(29) (X_{C4} = 27%, STY = 58 mg $g_{cat}^{-1}\ h^{-1}$, Fig. 5). The best-performing zeotype was hZSM-5(20)-PZSi, which led to X_{C4} = 77% and STY = 791 mg $g_{cat}^{-1}\ h^{-1}$, with the predominance of DCut products (mass ratio of DCut:NCut = 2.1 and STY_{DCut} = 534 mg $g_{cat}^{-1}\ h^{-1}$, TOS = 7 h).

The overall reaction mechanism of these systems may be very complex, involving for example, primary/secondary cracking and alkylation reactions, besides isomerisation (e.g. double bond or methyl shifts) and oligomerisation [64]. The relative amount of aromatic products (H_{ar}) and the isoparaffinic ratio (*I*), which reflects

Table 3
Al-species and acid properties of the MFI-based materials.

Sample	Al species[a]		Acid properties[b]			
	$\%Al_{tetra}$	$\%Al_{octa}$	L + B (μmol g^{-1})	L/B	L_{450}/L_{200}	B_{450}/B_{200}
hZSM-5(31)-noT	91	9	252	0.19	1.01	0.25
hZSM-5(20)-PZSi	75	25	251	1.34	0.47	0.06
hZSM-5(51)-PZSi	81	19	132	0.59	0.61	0.04
hZSM-5(47)-PZSiS	93	7	147	0.33	0.59	0.04
hZSM-5(31)-CoT	88	12	152	0.26	1.02	0.14
ZSM-5(29)	94	6	365	0.22	0.85	0.21

[a] Determined by ^{27}Al MAS NMR spectroscopy.
[b] Determined by FT-IR of pyridine adsorbed at 200 °C; B = Brönsted acid sites, L = Lewis acid sites, B + L = total amount of acid sites.

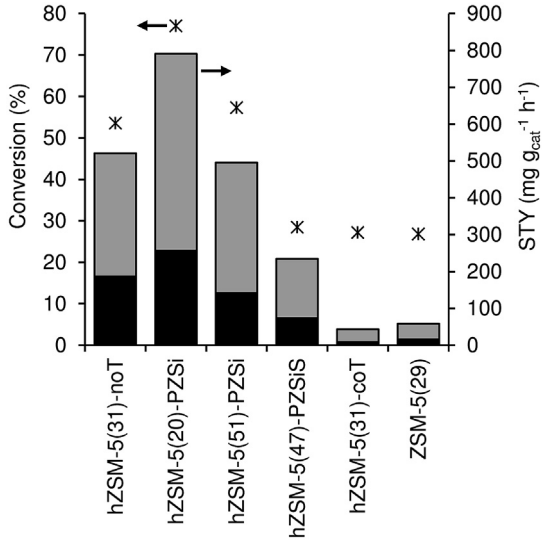

Fig. 5. Conversion (*) and STY (bars) of NCut (dark colour) and DCut (light colour) products for the MFI-based materials prepared and the benchmark catalyst ZSM-5(29). Reaction conditions: 200 °C, 30 bar, WHSV = 2.2 g_{1C4} g_{cat}^{-1} h^{-1}, TOS = 7 h, catalyst activation temperature = 450 °C.

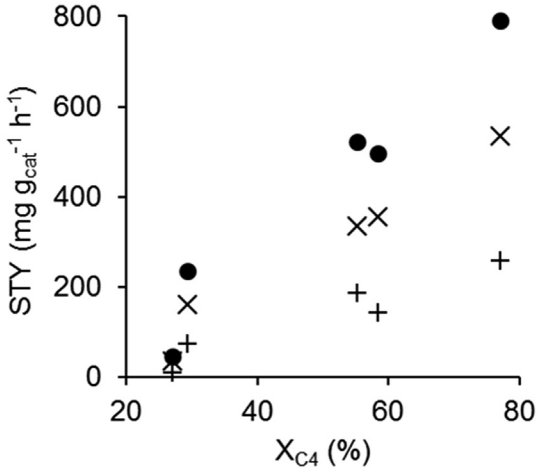

Fig. 7. STY as a function of X_{C4} for the different catalysts prepared (STY total (●), STY_{DCut} (×), and STY_{NCut} (+)). Reaction conditions: 200 °C, 30 bar, WHSV = 2.2 g_{1C4} g_{cat}^{-1} h^{-1}, TOS = 7 h, catalyst activation temperature = 450 °C.

the degree of branching of the liquid products, were determined by ^1H NMR spectroscopic analysis of the liquid reaction products (details in the Supplementary Material). For all materials, H_{ar} < 0.2%, indicating very low aromatics content. The low aromatics content and the absence of heteroatoms are advantages of light olefin oligomerisation routes for synthesising clean fuels. The *I* values were in the range 0.47–0.59, based on the O'Connor or Kapur methods [65,66]. These results are advantageously lower than that reported in the literature for a mesostructured zeotype based on the BEA topology (*I* ≈ 0.62) [57], tested under similar 1C4 reaction conditions. An estimation of the cetane number (CN, based on the O'Connor method [65]) indicated values in the range 43–50 (noteworthy, without post-treatments such as hydrogenation that

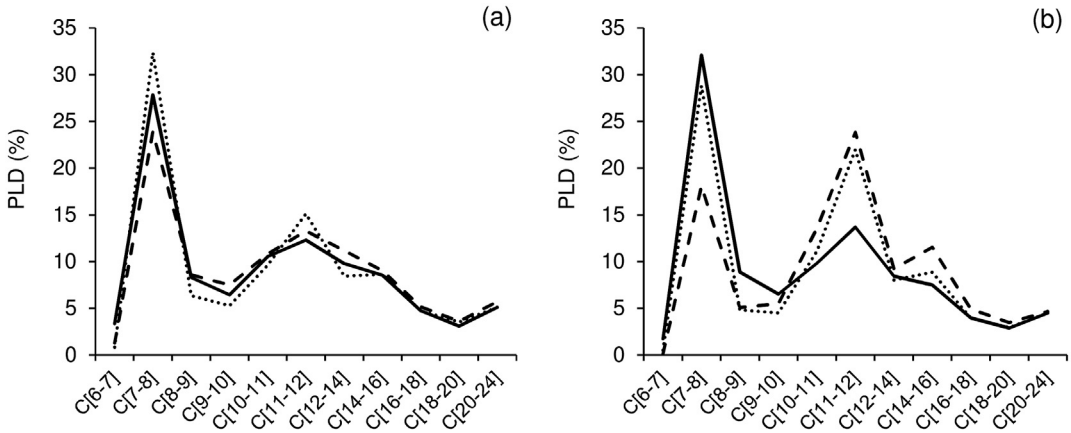

Fig. 6. PLD profiles for the liquid products of the reaction of 1-butene in the presence of the MFI-based materials: (a) hZSM-5(20)-PZSi (solid line), hZSM-5(51)-PZSi (dashed line), hZSM-5(47)-PZSiS (dotted line), and (b) hZSM-5(31)-noT (solid line), hZSM-5(31)-CoT (dashed line), and ZSM-5(29) (dotted line). Reaction conditions: 200 °C, 30 bar, WHSV = 2.2 g_{1C4} g_{cat}^{-1} h^{-1}, TOS = 7 h, catalyst activation temperature = 450 °C.

Table 4
Influence of the catalyst activation temperature (T_{act}) and reaction conditions (T, P) on the catalytic reaction.

Conditions			X_{C4} (%)	STY (mg. g^{-1} h^{-1})			DCut/NCut
T_{act} (°C)	T (°C)	P (bar)		NCut	DCut	Total	
200	200	30	77	272	543	815	2.0
450	200	30	77	257	534	791	2.1
450	250	30	87	414	611	1025	1.5
450	250	40	97	408	669	1077	1.6

increase the CN [67]). Literature data for CN of diesel cuts produced in commercial processes, and commercial diesel samples were in the range 48–56 [28,66,68–70].

The most active catalyst hZSM-5(20)-PZSi was further tested under different reaction conditions (Table 4). The catalyst activation temperature (T_{act}) of 200 °C or 450 °C prior to the oligomerisation reaction led to comparable catalytic results (similar X_{C4} and STY at 200 °C, 30 bar). Different results were reported in the literature for micro-mesoporous zeotypes based on the BEA topology, for which higher T_{act} led to poorer catalytic results; T_{act} may affect the coordination environment (and configuration) of the Al species of the BEA framework [57]. Conversion and STY increased with increasing reaction temperature from 200 to 250 °C, whereas the mass ratio DCut/NCut decreased from 2.1 to 1.5. Hence, the total productivity may be favoured by increasing the temperature, albeit the relative amount of DCut products decreases, which is consistent with the fact that the oligomerisation reaction is exothermic. Increasing the reaction pressure from 30 to 40 bar led to enhanced X_{C4} (87 and 97%, respectively) and STY_{DCut} (611 and 669 mg g_{cat}^{-1} h^{-1}, respectively) at 250 °C. These results are consistent with the fact that oligomerisation leads to reduction in the total number of molecules in the reaction system, and thus may be favoured with increased pressure.

The results for the best-performing catalyst hZSM-5(20)-PZSi (X_{C4} = 77%, STY = 791 mg g_{cat}^{-1} h^{-1}, mass ratio DCut/NCut = 2.1) compare favourably to literature data for several types of aluminosilicates, tested under similar 1C4 reaction conditions (200 °C. 30 bar): mesoporous aluminosilicates possessing amorphous pore walls [24]; versions of (large-pore) zeolite Beta such as, microcrystalline or nanocrystalline zeolite Beta [57]; and a composite of BEA nanocrystals embedded in a mesoporous siliceous matrix (Table S1) [57]. Interesting results were reported for a hierarchical zeotype based on the BEA topology (T_{act} = 200 °C) which led to X_{C4} (54%), and STY of 502 mg g_{cat}^{-1} h^{-1}, and commercial zeolite ZSM-5 with Si/Al = 15 (T_{act} = 450 °C) which led to X_{C4} = 39% and STY = 523 mg g_{cat}^{-1} h^{-1} [24,57]. Several studies reported 1C4 conversion over commercial ZSM-5, under different reaction conditions; one of the best results in terms of selectivity to diesel products was reported by Schwarz et al. [71], specifically, 76 wt% diesel selectivity at 99% 1C4 conversion (conversion of total butenes not specified), at 270 °C, 50 bar (Table S1). Under roughly comparable temperature and pressure conditions to those used by Schwarz et al., Li et al. [72] reported the conversion of butene (isomer not specified), over a ZSM-5 type material synthesised hydrothermally using hemicellulose, the initiator ammonium persulphate and tetramethylethylenediamine, which led to 88% diesel selectivity at 91% conversion, 40 bar, 270 °C (WHSV = 4.8 g_{1C4} g_{cat}^{-1} h^{-1}) (Table S1); this material possessed 17% S_{meso} and 33% V_{micro}

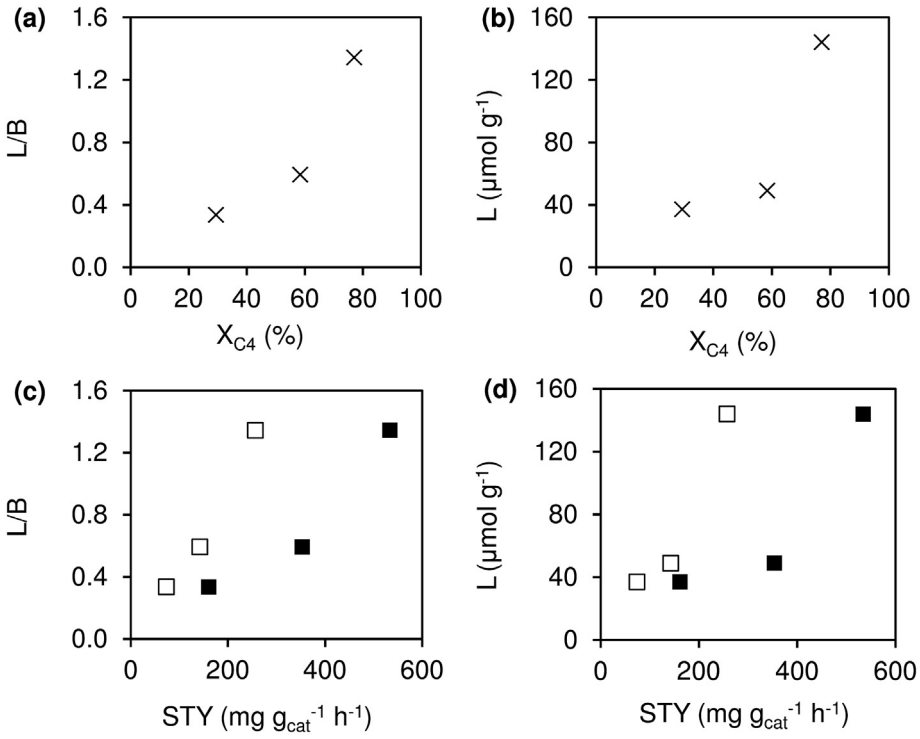

Fig. 8. Influence of the acid properties measured at 200 °C on X_{C4} (×), (a, b), STY_{DCut} (■) and STY_{NCut} (□) (c, d), for the catalysts prepared according to the PZSi(S) protocols, namely hZSM-5(20)-PZSi, hZSM-5(51)-PZSi, and hZSM-5(47)-PZSiS. Reaction conditions: 200 °C, 30 bar, WHSV = 2.2 g_{1C4} g_{cat}^{-1} h^{-1}, TOS = 7 h, catalyst activation temperature = 450 °C.

compared to 13% S_{meso} and 38% V_{micro} for ZSM-5 prepared in a conventional fashion, which together with the higher amount of total acid sites of the former, led to improved catalytic performance in relation to the conventional zeolite [72].

3.2.2. Influence of material properties

Conversion followed the order (X_{C4}): hZSM-5(31)-CoT (27%) ≈ hZSM-5(47)-PZSiS (28%) < hZSM-5(31)-noT (54%) ≈ hZSM-5(51)-PZSi (57%) < hZSM-5(20)-PZSi (77%). On the other hand, the total STY followed the order (mg g_{cat}^{-1} h^{-1}): hZSM-5(31)-CoT (43) < hZSM-5(47)-PZSiS (235) < hZSM-5(51)-PZSi (496) < hZSM-5(31)-noT (521) < hZSM-5(20)-PZSi (791). Direct relationships between the catalytic activity and the textural or acid properties could not be clearly established considering all materials at once. The catalytic performance may result from complex interplay of several properties including morphology, texture and acidity, which, in turn, depend on the synthesis protocol. It is important to reduce the number of variables in comparative studies to gain insights into structure-activity relationships. The materials prepared via the protocols CoT and noT possess the same molar ratio Si/Al (31) and roughly comparable S_{meso} (140 and 168 m^2 g^{-1}, respectively), Table 3. Yet, their catalytic performances were very different, with hZSM-5(31)-noT performing far superiorly to hZSM-5(31)-CoT; X_{C4} of 54 and 27%, and STY of 522 and 43 mg g_{cat}^{-1} h^{-1}, respectively. Zeotype hZSM-5(31)-noT possessed more regular morphology (Fig. 3), lower V_{micro} and higher amount of acid sites (Table 3) than hZSM-5(31)-CoT, which may result in a higher amount of effective (accessible) active sites in the former case, favouring the oligomerisation reaction.

Zeolite ZSM-5(29) possessed highest amount of acid sites, albeit its catalytic activity was similar to the least active material prepared namely hZSM-5(31)-CoT. The larger crystallite sizes (micron range) and relatively low S_{meso} of ZSM-5(29) may account for longer diffusional pathways and important steric hindrance effects. Hence, nanocrystals, mesoporosity and regular morphology seem important features to meet superior catalytic performances.

The materials based on the PZSi synthetic approach consisted of pseudo-spherical aggregates of nanocrystallites of 10–60 nm in size, and possessed comparable V_p, V_{micro} and S_{meso} (275–308 m^2 g^{-1}) and acid strengths. However, their catalytic performances were different, which seemed to be related to the relative amount of Lewis acid sites. Specifically, X_{C4} and STY

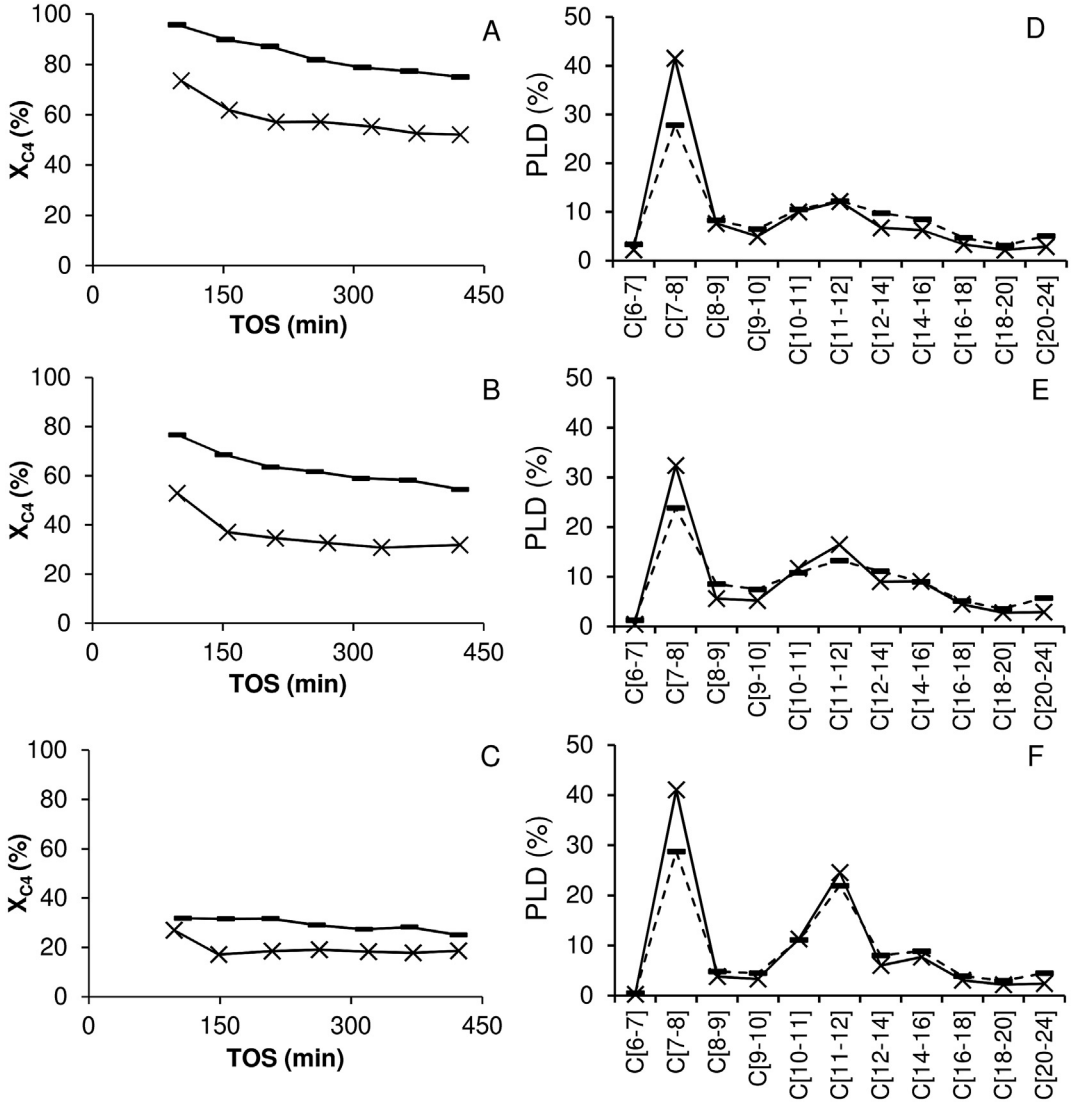

Fig. 9. Dependence of conversion (X_{C4}) on TOS for hZSM-5(20)-PZSi (A), hZSM-5(51)-PZSi (B) and ZSM-5(29) (C) in the first (×) and second cycle using the regenerated catalyst (−). PLD curves for the two cycles (with matching symbols) for hZSM-5(20)-PZSi (D), hZSM-5(51)-PZSi (E) and ZSM-5(29) (F).

increased with L/B, being highest for hZSM-5(20)-PZSi (Fig. 8). Thus, the Lewis acidity seemed favourable for the catalytic reaction. These results are in agreement with literature data for the oligomerisation of C4 olefins; e.g. 1C4 conversion over zeotypes possessing BEA topology [57], and isobutene conversion over commercial zeolite Beta [73], dealuminated zeolite Y or zeolite Y-supported $AlCl_3$ [42,74]. Since the material properties requirements may be different for olefins of different carbon chain lengths [37], comparisons have been restricted to C4 olefins. The post-synthesis surfactant treatment of hZSM-5(51)-PZSi gave hZSM-5(47)-PZSiS, which did not lead to improved X_{C4} or STY (Fig. 5); these results may be partly due to the lower L/B of hZSM-5(47)-PZSiS (Table 3).

Overall, the noT and PZSi synthetic strategies seem promising for preparing zeotype catalysts for olefin oligomerisation. One of the parameters that may be varied in all synthesis protocols is the Si/Al ratio, which may influence the acid properties of the final materials. The material prepared via the noT protocol (Si/Al = 31) possessed intermediate Si/Al ratio of the two PZSi based materials (20–51). Nevertheless, hZSM-5(31)-noT resembled somewhat closely the catalytic performance of hZSM-5(51)-PZSi and was outperformed by hZSM-5(20)-PZSi. The PZSi protocol seems to advantageously give materials with enhanced L/B ratio and S_{meso} for butene oligomerisation.

3.2.3. Catalytic stability

The catalyst stabilities of hZSM-5(20)-PZSi and hZSM-5(51)-PZSi were investigated, and compared to zeolite ZSM-5(29), at 200 °C, 30 bar. The originally pristine white solid catalysts turned brown in colour after the catalytic reaction. The carbon content of the washed/dried catalysts was ca. 13 wt% C (based on elemental analysis). DSC analysis of the used catalysts under air atmosphere indicated an endothermic process occurring at temperature lower than 200 °C, which was likely the desorption of physisorbed water and other volatiles (exemplified for hZSM-5(20)-PZSi in Fig. S6). Additionally, an exothermic process with an onset at ca. 280 °C occurred for the used catalysts, but not for the unused ones. The exothermic process was likely the combustion of coke deposits. The catalysts were regenerated by the thermal treatment at 550 °C and turned off-white in colour, suggesting that most of the coke was removed.

The regenerated catalysts were characterised in what regards the morphology (SEM, TEM), composition (EDS), crystal structure (PXRD), textural properties (N_2 adsorption), surface Al species (^{27}Al MAS NMR) and acid properties (FT-IR spectroscopy of adsorbed pyridine). For the three catalysts, the MFI crystalline structure was essentially preserved during the catalytic process (Fig. 9), and the morphology (Fig. S7) and textural properties remained similar (Table S2). For the zeotypes, the Si/Al ratio remained roughly constant, and molecular level characterization studies indicated the predominance of Al_{tetra} species and comparable L/B ratio (Table S3). The most pronounced difference was slight decrease of L + B for the used catalyst hZSM-5(20)-PZSi. The commercial zeolite ZSM-5(29) suffered drop in the Si/Al ratio, $\%Al_{tetra}$ and L + B, which was accompanied by the appearance of five-coordinated Al species (peak at ca. 25 ppm due to Al_{penta}) and slight increase in L/B. Based on the results regarding the material properties, the zeotypes seemed more stable than the zeolite.

The catalysts were used for two consecutive 7 h-on stream runs, with an intermediate step of catalyst regeneration. From the first to the second run it was verified partial catalyst deactivation, which was more pronounced for the zeotypes (X_{C4} at TOS = 7 h decreased by a factor of ca. 1.44) than ZSM-5(29) (X_{C4} decreased by a factor of ca. 1.4) (Fig. 10). The drop in activity of ZSM-5(29) somewhat correlated with the changes in surface Al_{tetra} species and acid properties of the used catalyst (discussed above). For the zeotypes, the partial catalyst deactivation did not correlate with the characterization results (which indicated that the physicochemical properties of the materials were fairly well preserved, especially in the case of hZSM-5(51)-PZSi).

The MFI based materials possess crystallographically different Al species, for which the intrinsic activity and stability may be different. Molecular-level changes may occur during the catalytic process, which are difficult to track by the characterization studies of the solids recovered after the catalytic reaction. Although the original and used zeotypes exhibited similar ^{27}Al MAS NMR spectra, it is important to consider that there may exist “NMR-invisible” Al species [75–77]. Woolery et al. [56] reported for MFI zeolites that treatment at high temperature may lead to the hydrolysis of Al-O bonds (e.g. less stable Al species subjected to local stress in a confined environment) and the formation of “NMR-invisible” Al

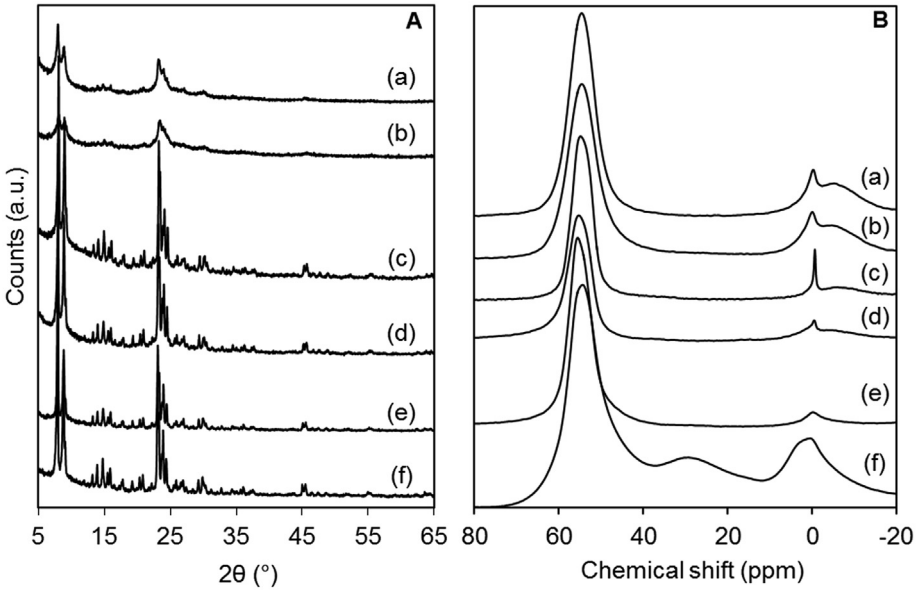

Fig. 10. PXRD patterns (A) and ^{27}Al MAS NMR spectra (B) for hZSM-5(20)-PZSi (fresh (a); used (b)), hZSM-5(51)-PZSi (fresh (c); used (d)), and ZSM-5(29) (fresh (e); used (f)).

species of Lewis type. The extent of the hydrolysis of the framework species may increase with temperature [75]. Accordingly, the temperature may affect the catalyst stability. The Al_{tetra} species may undergo hydrolysis to give framework-bonded Al_{octa} species; however, the latter may react reversibly to give Al_{tetra} species by the interaction with base molecules such as pyridine [75], which was used as probe for measuring the acid properties. Hence, although the molecular-level characterization studies based on the spectroscopic techniques ^{27}Al MAS NMR and FT-IR of adsorbed pyridine gave similar results for the original and used hZSM-5(51)-PZSi catalysts, for example, this does not rule out the possibility of occurring in situ changes of surface species; it is not trivial to track these possible modifications, and assess the intrinsic activities and relative amounts of the in situ modified surface species in order to study their influence on the catalytic reaction.

4. Conclusions

Non-destructive bottom-up synthetic approaches led to MFI-based zeotype catalysts with favourable morphological, textural and acid properties for olefin oligomerisation to higher molar mass products, under high pressure continuous flow conditions. In general, the zeotypes consisting of morphologically regular aggregates of nanocrystallites and possessing mesoporosity outperformed microcrystalline zeolite ZSM-5 in 1-butene oligomerisation, at 200 °C, 30 bar (even though the zeolite possessed the highest amount of total acid sites). The best performing zeotype was hZSM-5(20)-PZSi (Si/Al = 20), prepared via the Serrano et al. [46–48] strategy (PZSi) based on the crystallization of silanized protozeolitic units; 77% conversion of butenes, average space time yield of liquid products of 791 mg g_{cat}^{-1} h^{-1} (7 h on-stream) and mass ratio DCut/NCut = 2. These results compared favourably to literature data for several aluminosilicates tested under similar 1-butene oligomerisation reaction conditions. The materials prepared via the PZSi approach seemed to benefit from enhanced mesoporosity and L/B ratio for butene oligomerisation.

Characterization studies indicated that the morphology, structure, composition, textural and acid properties of the zeotypes were essentially preserved during the catalytic reaction and the catalyst regeneration processes. Molecular-level characterization of the zeotypes and the zeolite, suggested superior stability of the former in what concerns the Al-species and acid properties. However, partial drop in catalytic activity was verified for the regenerated catalysts, possibly due to changes in surface chemical properties occurring in situ, under the operating conditions. It is not trivial to track these changes by characterization studies of the catalysts recovered after the reaction. While envisaging zeotypes as promising catalysts for olefin oligomerisation, important future challenges include in situ high temperature characterization studies to track possible changes in surface chemical species occurring under the operating conditions, and gain more insights into effective structure-activity relationships, which may aid in the improvement of material properties to meet superior performances.

Declarations of interest

None.

Acknowledgements

This work was developed in the scope of the project CICECO-Aveiro Institute of Materials, FCT (Fundação para a Ciência e Tecnologia) Ref. UID/CTM/50011/2019, financed by national funds through the FCT/MCTES. The FCT and the European Union are acknowledged for a Ph.D. grant to A.F.S. (SFRH/BD/101018/2014). M.M.A. and A.F. thank the costs resulting from the FCT hirings which are funded by national funds (OE), through FCT – Fundação para a Ciência e a Tecnologia , I.P., in the scope of the framework contract foreseen in the numbers 4, 5 and 6 of the article 23, of the Decree-Law 57/2016, of August 29, changed by Law 57/2017, of July 19. The authors wish to thank Saint-Gobain Ceramic Materials AS for generously supplying the SIKA SiC sample.

Appendix A. Supplementary data

Supplementary data to this article can be found online at https://doi.org/10.1016/j.renene.2019.02.019.

References

[1] U.S. Administration, Energy Information. International Energy Outlook, 2016. https://www.eia.gov/outlooks/ieo/pdf/0484(2016).pdf. (Accessed 20 May 2018).
[2] U.S. Administration, Energy Information. International Energy Outlook, 2017. https://www.eia.gov/outlooks/ieo/pdf/0484(2017).pdf. (Accessed 20 May 2018).
[3] E. Kriván, I. Valkai, J. Hancsók, Investigation of production of motor fuel components on heterogeneous catalyst with oligomerization, Top. Catal. 56 (2013) 831–838.
[4] G. Bellussi, F. Mizia, V. Calemma, P. Pollesel, R. Millini, Oligomerization of olefins from Light Cracking Naphtha over zeolite-based catalyst for the production of high quality diesel fuel, Microporous Mesoporous Mater. 164 (2012) 127–134.
[5] M.A. Maseloane, Dimerization of naphtha-range Fischer-Tropsch olefins into diesel-range products over zeolite H-ZSM-5 and amorphous silica-alumina, University of Cape Town, South Africa, 2011.
[6] A. De Klerk, Distillate production by oligomerization of Fischer-Tropsch olefins over solid phosphoric acid, Energy Fuels 20 (2006) 439–445.
[7] J.Q. Bond, D.M. Alonso, D. Wang, R.M. West, J.A. Dumesic, Integrated catalytic conversion of γ-valerolactone to liquid alkenes for transportation fuels, Science 327 (2010) 1110–1114.
[8] J.Q. Bond, A.A. Upadhye, H. Olcay, G.A. Tompsett, J. Jae, R. Xing, et al., Production of renewable jet fuel range alkanes and commodity chemicals from integrated catalytic processing of biomass, Energy Environ. Sci. 7 (2014) 1500–1523.
[9] D.M. Alonso, J.Q. Bond, J.C. Serrano-Ruiz, J.A. Dumesic, Production of liquid hydrocarbon transportation fuels by oligomerization of biomass-derived C9 alkenes, Green Chem. 12 (2010) 992–999.
[10] C.P. Nicholas, Applications of light olefin oligomerization to the production of fuels and chemicals, Appl. Catal. Gen. 543 (2017) 82–97.
[11] A. Corma, S. Iborra, Oligomerization of alkenes, in: E.G. Derouane (Ed.), Catalysts for Fine Chemical Synthesis, vol. 4, Microporous Mesoporous Solid Catalysts, John Wiley & Sons, 2006, pp. 125–140.
[12] M. Sanati, C. Hörnell, S.G. Järås, The Oligomerization of Alkenes by Heterogeneous Catalysts, in: J.J. Spivey (Ed.), Catalysis, vol. 14, The Royal Society of Chemistry, Cambridge, 1999, pp. 236–287.
[13] O. Muraza, Maximizing diesel production through oligomerization: a landmark opportunity for zeolite research, Ind. Eng. Chem. Res. 54 (2015) 781–789.
[14] J. Weitkamp, S. Ernst, L. Puppe, Shape-selective catalysis, in: J. Weitkamp, L. Puppe (Eds.), Zeolites. Catalysis and Zeolites. Fundamentals and Applications, Springer-Verlag Berlin Heidelberg, New York, 1999, pp. 327–376.
[15] C.H. Christensen, K. Johannsen, E. Törnqvist, I. Schmidt, H. Topsøe, C.H. Christensen, Mesoporous zeolite single crystal catalysts: Diffusion and catalysis in hierarchical zeolites, Catal. Today 128 (2007) 117–122.
[16] M.S. Holm, E. Taarning, K. Egeblad, C.H. Christensen, Catalysis with hierarchical zeolites, Catal. Today 168 (2011) 3–16.
[17] J. Weitkamp, Zeolites and catalysis, Solid State Ionics 131 (2000) 175–188.
[18] P.M.M. Blauwhoff, J.W. Gosselink, E.P. Kieffer, S.T. Sie, W.H.J. Stork, Zeolites as Catalysts in Industrial Processes, in: J. Weitkamp, L. Puppe (Eds.), Catalysis and Zeolites, Springer Berlin Heidelberg, Berlin, 1999, pp. 437–538.
[19] J. Cejka, H. Van Bekkum, Zeolites and Ordered Mesoporous Materials: Progress and Prospects, first ed., vol. 157, Elsevier Science, 2005.
[20] A. Corma, From microporous to mesoporous molecular sieve materials and their use in catalysis, Chem. Rev. 97 (1997) 2373–2419.
[21] B. Chiche, E. Sauvage, F. Di Renzo, I.I. Ivanova, F. Fajula, Butene oligomerization over mesoporous MTS-type aluminosilicates, J. Mol. Catal. Chem. 134 (1998) 145–157.
[22] J.P.G. Pater, P.A. Jacobs, J.A. Martens, Oligomerization of hex-1-ene over acidic aluminosilicate zeolites, MCM-41, and silica-alumina co-gel catalysts: A comparative study, J. Catal. 184 (1999) 262–267.
[23] Y. Tao, H. Kanoh, L. Abrams, K. Kaneko, Mesopore-modified zeolites: Preparation, characterization, and applications, Chem. Rev. 106 (2006) 896–910.
[24] A.F. Silva, A. Fernandes, M.M. Antunes, P. Neves, S.M. Rocha, M.F. Ribeiro, et al.,

TUD-1 type aluminosilicate acid catalysts for 1-butene oligomerisation, Fuel 209 (2017) 371–382.
[25] J.T.F. Degnan, Applications of zeolites in petroleum refining, Top. Catal. 13 (2000) 349–356.
[26] N.V. Choudary, B.L. Newalkar, Use of zeolites in petroleum refining and petrochemical processes: recent advances, J. Porous Mater. 18 (2011) 685–692.
[27] S.A. Tabak, F.J. Krambeck, A.A. Avidan, Production of synthetic gasoline and diesel fuel from non-petroleum resources, Am. Chem. Soc. Div. Gas Fuel Chem. 31 (1986) 293–299.
[28] C. Knottenbelt, Mossgas "gas-to-liquid" diesel fuels - an environmentally friendly option, Catal. Today 71 (2002) 437–445.
[29] R.O. Minnie, Catalytic conversion of olefins to diesel and gasoline fuel, 2006. WO 2006091986 A1.
[30] A de Klerk, E. Furimsky, Catalysis in the Upgrading of Fischer–Tropsch Syncrude, in: E. Furimsky (Ed.), Catalysis in the Refining of Fischer–Tropsch Syncrude, Royal Society of Chemistry, Cambridge, 2010, pp. 40–164.
[31] A.V. Lavrenov, T.R. Karpova, E.A. Buluchevskii, E.N. Bogdanets, Heterogeneous oligomerization of light alkenes: 80 years in oil refining, Catal. Ind. 8 (2016) 316–327.
[32] M.J. Wulfers, R.F. Lobo, Assessment of mass transfer limitations in oligomerization of butene at high pressure on H-beta, Appl. Catal. Gen. 505 (2015) 394–401.
[33] D.P. Serrano, J.M. Escola, P. Pizarro, Synthesis strategies in the search for hierarchical zeolites, Chem. Soc. Rev. 42 (2013) 4004–4035.
[34] R. Chal, C. Gérardin, M. Bulut, S. van Donk, Overview and industrial assessment of synthesis strategies towards zeolites with mesopores, ChemCatChem 3 (2011) 67–81.
[35] K. Zhu, X. Zhou, Manipulating the architecture of zeolite catalysts for enhanced mass transfer, Curr. Opin. Chem. Eng. 9 (2015) 42–48.
[36] J. Pérez-Ramírez, C.H. Christensen, K. Egeblad, C.H. Christensen, J.C. Groen, Hierarchical zeolites: enhanced utilisation of microporous crystals in catalysis by advances in materials design, Chem. Soc. Rev. 37 (2008) 2530–2542.
[37] A. Corma, C. Martínez, E. Doskocil, Designing MFI-based catalysts with improved catalyst life for C3= and C5= oligomerization to high-quality liquid fuels, J. Catal. 300 (2013) 183–196.
[38] X. Wang, X. Hu, C. Song, K.W. Lux, M. Namazian, T. Imam, Oligomerization of biomass-derived light olefins to liquid fuel: effect of alkali treatment on the HZSM-5 catalyst, Ind. Eng. Chem. Res. 56 (2017) 12046–12055.
[39] N.A.S. Amin, D.D. Anggoro, Dealuminated ZSM-5 zeolite catalyst for ethylene oligomerization to liquid fuels, J. Nat. Gas Chem. 11 (2002) 79–86.
[40] C. Bertrand-Drira, X-wei Cheng, T. Cacciaguerra, P. Trens, G. Melinte, O. Ersen, et al., Mesoporous mordenites obtained by desilication: Mechanistic considerations and evaluation in catalytic oligomerization of pentene, Microporous Mesoporous Mater. 213 (2015) 142–149.
[41] M.J. Van Niekerk, C.T. O'Connor, J.C.Q. Fletcher, Methanol conversion and propene oligomerization productivity of dealuminated large-port mordenites, Ind. Eng. Chem. Res. 35 (1996) 697–702.
[42] J.W. Yoon, S.H. Jhung, D.H. Choo, S.J. Lee, K.-Y. Lee, J.-S. Chang, Oligomerization of isobutene over dealuminated Y zeolite catalysts, Appl. Catal. Gen. 337 (2008) 73–77.
[43] C. Martínez, E.J. Doskocil, A. Corma, Improved THETA-1 for light olefins oligomerization to diesel: influence of textural and acidic properties, Top. Catal. 57 (2014) 668–682.
[44] L. Wang, Z. Zhang, C. Yin, Z. Shan, F.-S. Xiao, Hierarchical mesoporous zeolites with controllable mesoporosity templated from cationic polymers, Microporous Mesoporous Mater. 131 (2010) 58–67.
[45] Q. Yang, H. Zhang, M. Kong, X. Bao, J. Fei, X. Zheng, Hierarchical mesoporous ZSM-5 for the dehydration of methanol to dimethyl ether, Chin. J. Catal. 34 (2013) 1576–1582.
[46] D.P. Serrano, J.M. Escola, R. Sanz, R.A. Garcia, A. Peral, I. Moreno, et al., Hierarchical ZSM-5 zeolite with uniform mesopores and improved catalytic properties, New J. Chem. 40 (2016) 4206–4216.
[47] D.P. Serrano, J. Aguado, G. Morales, J.M. Rodríguez, A. Peral, M. Thommes, et al., Molecular and meso- and macroscopic properties of hierarchical nanocrystalline ZSM-5 zeolite prepared by seed silanization, Chem. Mater. 21 (2009) 641–654.
[48] D.P. Serrano, J. Aguado, J.M. Escola, J.M. Rodríguez, A. Peral, Hierarchical zeolites with enhanced textural and catalytic properties synthesized from organofunctionalized seeds, Chem. Mater. 18 (2006) 2462–2464.
[49] Z. Wan, W. Wu, W. Chen, H. Yang, D. Zhang, Direct synthesis of hierarchical ZSM-5 zeolite and its performance in catalyzing methanol to gasoline conversion, Ind. Eng. Chem. Res. 53 (2014) 19471–19478.
[50] J.M. Campelo, F. Lafont, J.M. Marinas, Pt/SAPO-5 and Pt/SAPO-11 as catalysts for the hydroisomerization and hydrocracking of n-octane, J. Chem. Soc., Faraday Trans. 91 (1995) 1551–1555.
[51] X. Li, D. Han, H. Wang, G. Liu, B. Wang, Z. Li, et al., Propene oligomerization to high-quality liquid fuels over Ni/HZSM-5, Fuel 144 (2015) 9–14.
[52] A.S. Al-Dughaither, H. de Lasa, HZSM-5 zeolites with different SiO2/Al2O3 ratios. Characterization and NH3 desorption kinetics, Ind. Eng. Chem. Res. 53 (2014) 15303–15316.
[53] M.M.J. Treacy, J.B. Higgins, Collection of simulated XRD powder patterns for zeolites, fifth ed., Elsevier, 2007.
[54] K. Góra-Marek, M. Derewiński, P. Sarv, J. Datka, IR and NMR studies of mesoporous alumina and related aluminosilicates, Catal. Today 101 (2005) 131–138.
[55] J.M.R. Gallo, C. Bisio, G. Gatti, L. Marchese, H.O. Pastore, Physicochemical characterization and surface acid properties of mesoporous [Al]-SBA-15 obtained by direct synthesis, Langmuir 26 (2010) 5791–5800.
[56] G.L. Woolery, G.H. Kuehl, H.C. Timken, A.W. Chester, J.C. Vartuli, On the nature of framework Lewis acid sites in ZSM-5 Brarnsted and, Zeolites 2449 (1997) 288–296.
[57] A.F. Silva, A. Fernandes, P. Neves, M.M. Antunes, S.M. Rocha, M.F. Ribeiro, et al., Mesostructured catalysts based on the BEA topology for olefin oligomerisation, ChemCatChem 10 (2018) 2741–2754, https://doi.org/10.1002/cctc.201701597.
[58] Harandi MN, Owen H. Integrated staged conversion of methanol to gasoline and distillate. US 4899002 A, 1988.
[59] S.A. Tabak, F.J. Krambeck, W.E. Garwood, Conversion of propylene and butylene over ZSM-5 catalyst, AIChE J. 32 (1986) 1526–1531, https://doi.org/10.1002/aic.690320913.
[60] J.G. Yates, P.N. Rowe, S.T. Whang, The isomerization of n-butenes over a fluidised silica-alumina catalyst, Chem. Eng. Sci. 25 (1970) 1387–1394.
[61] M.L. Sarazen, E. Doskocil, E. Iglesia, Effects of void environment and acid strength on alkene oligomerization selectivity, ACS Catal. 6 (2016) 7059–7070.
[62] N. Kumar, P. Mäki-Arvela, T. Yläsalmi, J. Villegas, T. Heikkilä, A.R. Leino, et al., Dimerization of 1-butene in liquid phase reaction: Influence of structure, pore size and acidity of Beta zeolite and MCM-41 mesoporous material, Microporous Mesoporous Mater. 147 (2012) 127–134.
[63] W. Keim, B. Hoffmann, R. Lodewick, M. Peuckert, G. Schmitt, J. Fleischhauer, et al., Linear oligomerization of olefins via nickel chelate complexes and mechanistic considerations based on semi-empirical calculations, J. Mol. Catal. 6 (1979) 79–97.
[64] M. Henry, M. Bulut, W. Vermandel, B. Sels, P. Jacobs, D. Minoux, et al., Low temperature conversion of linear C4 olefins with acid ZSM-5 zeolites of homogeneous composition, Appl. Catal. Gen. 413–414 (2012) 62–77.
[65] C.T. O'Connor, R.D. Forrester, M.S. Scurrell, Cetane number determination of synthetic diesel fuels, Fuel 71 (1992) 1323–1327.
[66] G.S. Kapur, A. Ecker, R. Meusinger, Establishing quantitative structure-property relationships (QSPR) of diesel samples by proton-NMR & multiple linear regression (MLR) analysis, Energy Fuels 15 (2001) 943–948.
[67] A. de Klerk, Can Fischer-Tropsch syncrude be refined to on-specification diesel fuel? Energy Fuels 23 (2009) 4593–4604.
[68] H. de Lasa, G. Dogammau, A. Ravella, Fuels of the future and changing fuel needs, in: H. de Lasa, G. Dogammau, A. Ravella (Eds.), Reactor Technology for Environmentally Safe Reactors and Products, Springer Netherlands, 1992, pp. 1–182.
[69] D. Leckel, Diesel production from Fischer-Tropsch: the past, the present, and new concepts, Energy Fuels 23 (2009) 2342–2358.
[70] A. De Klerk, Fischer–Tropsch refining: technology selection to match molecules, Green Chem. 10 (2008) 1249–1279.
[71] S. Schwarz, M. Kojima, C.T. O'Connor, Effect of silicon-to-aluminium ratio and synthesis time on high-pressure olefin oligomerization over ZSM-5, Appl. Catal. 56 (1989) 263–280.
[72] C. Li, J. Du, H. Wang, X. Li, S.S. Zhu, G. Liu, et al., A hemicellulose modified HZSM-5 and their application in the light olefins oligomerization to high-quality liquid fuels reaction, Catal. Commun. 102 (2017) 89–92.
[73] J.W. Yoon, J.-S. Chang, H.-D. Lee, T.-J. Kim, S.H. Jhung, Trimerization of isobutene over a zeolite beta catalyst, J. Catal. 245 (2007) 253–256.
[74] J.W. Yoon, J.S. Lee, S.H. Jhung, K.-Y. Lee, J.-S. Chang, Oligomerization of isobutene over aluminum chloride-loaded USY zeolite catalysts, J. Porous Mater. 16 (2009) 631–634.
[75] L. Mafra, J.A. Vidal-Moya, T. Blasco, Structural Characterization of Zeolites by Advanced Solid State NMR Spectroscopic Methods, vol. 77, 2012.
[76] P.V. Wiper, J. Amelse, L. Mafra, Multinuclear solid-state NMR characterization of the Brønsted/Lewis acid properties in the BP HAMS-1B (H-[B]-ZSM-5) borosilicate molecular sieve using adsorbed TMPO and TBPO probe molecules, J. Catal. 316 (2014) 240–250.
[77] S. Hayashi, K. Jimura, N. Kojima, Microporous and Mesoporous Materials Acid property of MFI-type zeolites probed by trimethylphosphine oxide studied by solid-state NMR, Microporous Mesoporous Mater. 186 (2014) 101–105.